ISSN 0003-701X, Applied Solar Energy, 2023, Vol. 59, No. 3, pp. 189–200. © Allerton Press, Inc., 2023.

SOLAR ENGINEERING MATERIALS SCIENCE

Structure of Ag-Containing Cu_2ZnSnS_4 Thin Films, Obtained by Spray Pyrolysis

A. A. Zgliui[a], M. S. Tivanov[a, *], N. N. Curmei[b], L. V. Dermenji[b], L. I. Bruc[b], and D. A. Serban[b]

[a] *Faculty of Physics, Belarusian State University, Minsk, 220030 Belarus*

[b] *Institute of Applied Physics, Moldova State University, Chisinau, MD2028 Moldova*

**e-mail: michael.tivanov@gmail.com*

Received January 20, 2023; revised March 30, 2023; accepted May 2, 2023

Abstract—Kesterite Cu_2ZnSnS_4 thin films were synthesized by the spray pyrolysis method with subsequent annealing at temperatures in the range from 425 to 525°C. To understand the impact of Ag on the Cu_2ZnSnS_4 structural properties, changes in the elemental and phase composition, as well as microstructure were studied by electron microanalysis, X-ray phase and Raman analysis, scanning probe microscopy and scanning electron microscopy. The obtained samples have a compact morphology without appreciable voids and pores and crystallize in the tetragonal structure of kesterite CZTS. Phase analysis indicated incorporation of Ag in different concentrations without formation of other impurity compounds. An increase in the annealing temperature leads to an increase in the coherent scattering region, while the stoichiometric ratio of metals to chalcogen approaches 1, remaining close to that upon Ag alloying.

Keywords: Cu_2ZnSnS_4 thin films, spray pyrolysis, kesterite, structure, surface morphology

DOI: 10.3103/S0003701X23600790

INTRODUCTION

Among thin film materials, Cu_2ZnSnS_4 (CZTS) is one of the most promising light-absorbing materials due to its physical properties [1–3]—a high coefficient of optical absorption near the absorption edge (10^4 cm^{-1}), a band gap of 1.45 eV [1, 4–7]. In addition, CZTS is a p-type direct-gap semiconductor with a tetragonal crystal structure [8]. Moreover, from environmental and economic viewpoints, the use of CZTS is attractive because all of its constituent elements are rather abundant and none of them is harmful to the environment in the quantities used [9, 10].

The use of kesterite CZTS film in solar cells is possible both as an absorbing layer in CdS/CZTS heterostructures [11] for which an efficiency of 14.1% has been achieved, and in Cd-free solar cells with maximum efficiency of 10.3% [12]. In addition, CZTS layers also find application in the development of efficient and usable perovskite solar cells [13, 14]. In all cases, the weak point of CZTS is the presence of high density of structural defects, which hinder the creation of highly efficient solar cells. The addition of chemical elements like Ag, Cd, Ge can reduce the concentration of structural defects leading to improving the performance of solar cells produced using CZTS.

There are numerous synthesis methods suitable for CZTS thin films producing, most common of which are as follows:

— Ion plasma sputtering (offers sputtering of various alloys without changing their composition; however, with sputtering of this type, a strong heating of the substrate occurs and its material mixes with the film material) [15].

— Electrochemical deposition (attractive due to its low cost and thickness homogeneity of the obtained films; however, it is used only for metal films and sufficiently large amounts of impurities cause problems) [15].

— Pulsed laser deposition (good in terms of performance, hardware and design, but it depends on a large number of parameters such as repetition rate, drop power and substrate temperature) [16].

— Spray pyrolysis method (characterized by simplicity of implementation requires no complex equipment) [15–17].

— Magnetron sputtering method (physical vapor deposition technique used to synthesize thin films with good uniformity; regulation of such operating parameters as pressure, and the like allows one to control the film properties but the process of the method is highly energy intensive) [18].

As shown in the earlier studies, owing to the spray pyrolysis method, the composition of films can be easily controlled simply by changing the composition of the precursor solution [10]. Ag alloying is an effective strategy to change the carrier density of CZTS thin films and to suppress intrinsic harmful defects (e.g. Cu_{Zn} antisites), thus increasing the quality of the

Table 1. Percentage of the elements in Cu_2ZnSnS_4 films without Ag-alloying

T_{an}, °C	Cu, at %	Zn, at %	Sn, at %	S, at %	Stoichiometric ratio (Cu + Zn + Sn)/S
as deposited	25.7	16.4	19.3	38.7	1.59
425	22.6	14.7	17.5	45.2	1.21
475	22.3	14.9	18.8	44.0	1.27
525	21.0	13.7	16.8	48.5	1.06

obtained photovoltaic materials and improving the corresponding characteristics of solar cells [9, 19, 20].

The elemental composition and surface morphology of thin films affect their efficiency: deviation from the stoichiometric composition, high roughness of thin films, and their heterogeneity lead to a decrease in the efficiency of sunlight conversion.

Therefore, the purpose of this work is to determine the influence of the annealing temperature and the concentration of Ag alloying on the structure, elemental composition and morphology of Cu_2ZnSnS_4 thin films produced by spray pyrolysis.

In this work the spray pyrolysis method was chosen as the most suitable and inexpensive method for synthesis films. Also, CZTS thin films were annealed at temperatures 425, 475 and 525°C (were chosen as some average value of samples annealing temperatures most suitable for CZTS films) and alloyed with Ag at various concentrations $[C_{Ag}] = 1–3\%$ [21].

EXPERIMENTAL

Preparation of Cu_2ZnSnS_4 Thin Films

Deposition of thin layers of Ag-containing CZTS was carried out by the method of spray pyrolysis in an atmosphere of carbon dioxide at temperatures of 270–280°C. An oxygen-free atmosphere eliminates the oxidation reactions of the kesterite components during pyrolysis. The samples of CZTS films were formed on the molybdenum-coated SLG substrate. To increase the crystallinity of the films, annealing was carried out in a S_2 atmosphere at 425, 475 and 525°C for 30 min [22].

Characterization Details

The elemental composition of thin films was studied by X-ray energy dispersive spectroscopy (EDX) using an Quantax EDX attachment (Bruker) having energy spectral resolution of 125 eV and chemical element determining sensitivity of 0.1 at %.

The structural characteristics and phase composition of CZTS thin films were analyzed by X-ray phase analysis (XRD) using an Ultima IV X-ray diffractometer (Rigaku) in the grazing incidence (1°) X-ray diffraction geometry (GIXD) with a Cu$K\alpha$ radiation source ($\lambda = 0.15406$ nm) scanned in the range of 10° to 80° with a step of 0.05°. The phase composition of CZTS thin films was also studied by Raman analysis using a Nanofinder HE (LOTIS TII) confocal Raman spectrometer. To excite Raman radiation, a continuous-wave solid-state laser with the wavelength 532 nm was used. Raman measurements were carried out using laser radiation power of ~200 μW, laser spot diameter was of 0.6 μm, the spectral resolution was better than 3 cm^{-1}.

The surface structure was studied by scanning electron microscopy (SEM) using a VEGA 3 (Tescan) microscope in secondary electrons mode (accelerating voltage of 10 kV). The surface morphology was analyzed by atomic-force microscopy (AFM) using SolverNano (NT-MDT) microscope in the tapping mode with a silicon probe (at the tip radius 10 nm and the oscillation amplitude frequency 236 kHz), the lateral resolution was better than 40 nm and the vertical resolution was better than 1 nm.

RESULTS AND DISCUSSION

The results of EDX analysis are presented in Tables 1, 2 and on the typical EDX spectrum of the CZTS compound (Fig. 1).

As the annealing temperature T increases, one can observe a decrease in the amount of metals and an increase in the amount of sulfur S. Besides, the ratio (Cu + Zn + Sn)/S approximates the stoichiometric value equal to 1 (Table 1). The sample obtained at 475°C is slightly out of this trend, which can be explained by the fact that this sample has a smoother surface, as follows from the SEM and AFM data, analyzed below. Annealing is carried out in a S_2 atmosphere, and the sulfur adsorption process on the surface is more successful in the case of a rougher (developed) surface.

As seen, the samples are closest to the stoichiometry for the annealing temperature of 525°C. Therefore, this annealing temperature of thin films was used to analyze the effect on their structure and morphology with Ag-alloying at different concentrations (Table 2). Note that, with increase in the concentration of alloying with Ag, the stoichiometric ratio of metals to chalcogen remains close to 1.

The obtained SEM images of CZTS films deposited at different temperatures and Ag-alloying are

Table 2. Percentage of the elements in Cu_2ZnSnS_4 films annealed at 525°C

$[C_{Ag}]$, at %	Cu, at %	Zn, at %	Sn, at %	S, at %	Ag/(Ag + Cu) ratio	Stoichiometric ratio (Cu + Zn + Sn + Ag)/S
0.0	20.9	13.7	16.8	48.5	0.00	1.06
1.2	19.9	15.8	12.3	50.9	0.06	0.96
1.9	19.9	16.0	13.3	48.9	0.09	1.05
2.9	19.3	15.4	14.8	47.6	0.13	1.04

Table 3. Topographic parameters of Cu_2ZnSnS_4 thin films without alloying

T_{an}, °C	Average roughness R_a, μm	Root mean square roughness R_{rms}, μm	Skewness R_{sk}	Kurtosis R_{ku}
as deposited	0.20	0.27	0.75	5.35
425	0.21	0.27	0.91	3.83
475	0.13	0.19	1.60	9.52
525	0.23	0.29	0.38	3.12

shown in Fig. 2. It is demonstrated that thin films are solid and have no holes, voids or cracks on them. The thickness of all investigated films was about 1.6–1.9 μm, according to cross sectional SEM data.

The typical AFM images, made on an area of 20 × 20 μm, are shown in Fig. 3.

Scanning probe microscopy measurements enable one to calculate the topographic parameters of the film surface. The obtained data are given in Tables 3 and 4. The values obtained for R_a (arithmetic roughness) and R_{rms} (root mean square roughness), called the amplitude or height parameters, characterize the surface irregularity in the vertical direction. The parameter R_{sk} characterizes the symmetry of the profile with respect to the midline. The parameter R_{sk} is greater than 0 in all samples. This means that the surface of thin films reveals more high peaks than pits. The kurtosis coefficient $R_{ku} > 3$ indicates that the film surfaces have a leptocurtic distribution and have many high peaks and low pits. The sample with an annealing temperature of 525°C is closest to the symmetrical profile distribution about the midline (Table 3).

With an increase of the Ag-alloying concentration (Table 4), asymmetry of the films still has positive values. When the concentration of Ag equals 0 and 2.9%, the kurtosis $R_{ku} > 3$, so the surface has a lepto-

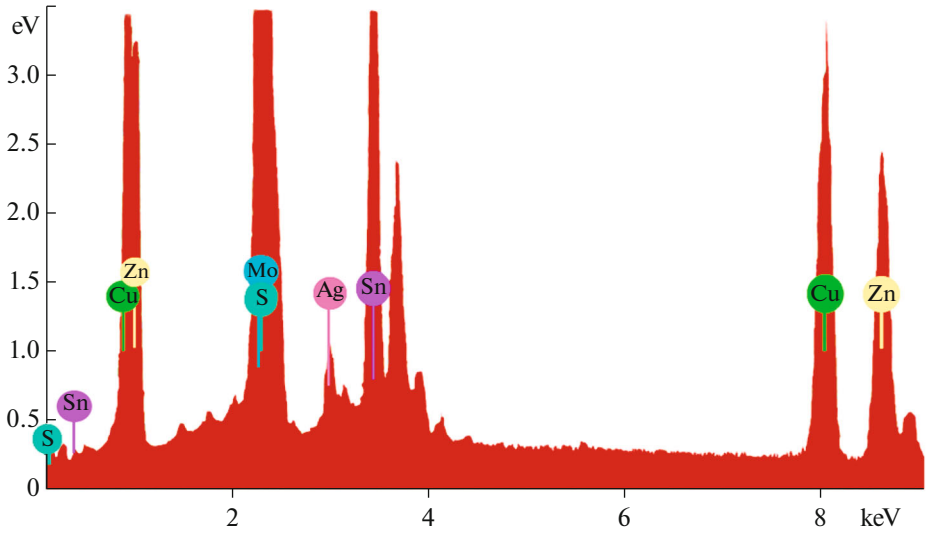

Fig. 1. Typical EDX spectrum of the Ag-alloyed (1.9%) Cu_2ZnSnS_4 thin films annealed at 525°C.

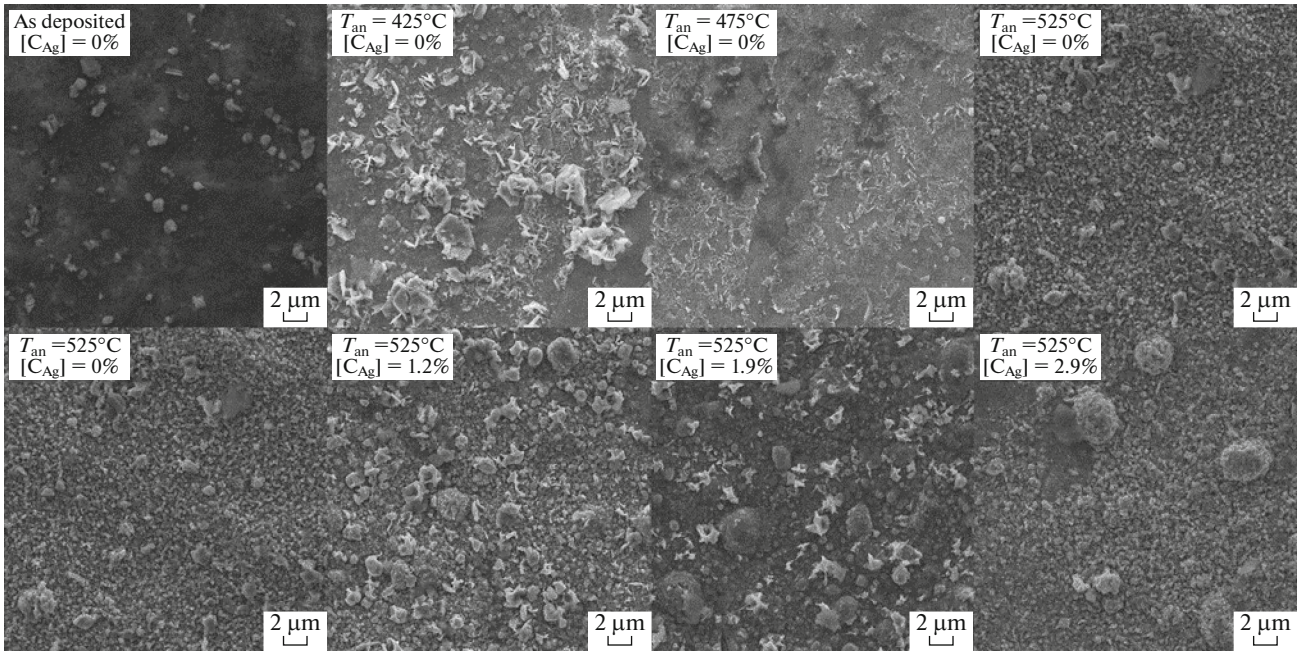

Fig. 2. Typical SEM images of Cu_2ZnSnS_4 films.

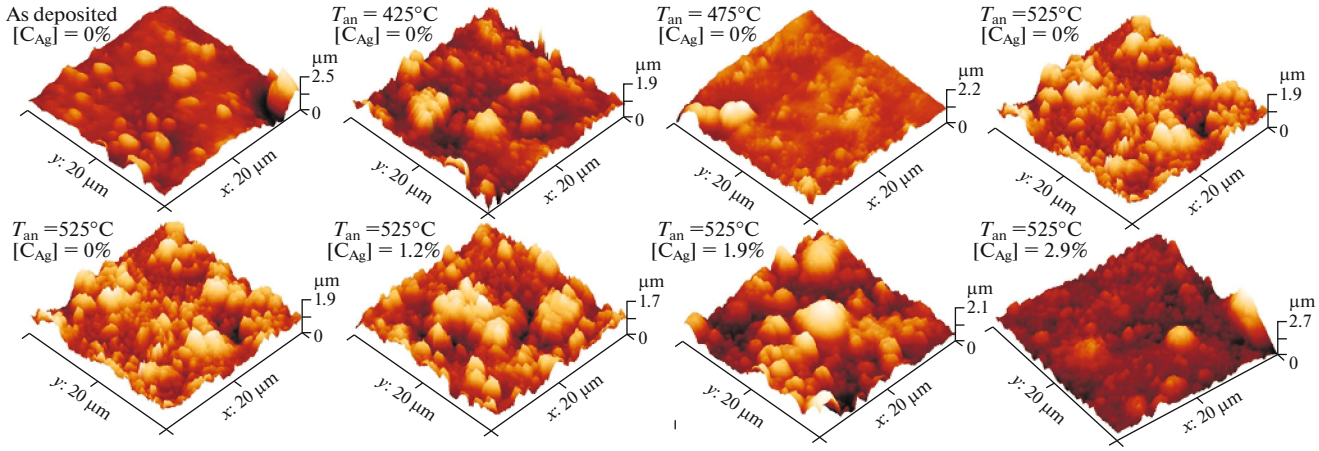

Fig. 3. Typical AFM images of Cu_2ZnSnS_4 films.

Table 4. Topographic parameters of Cu_2ZnSnS_4 thin films annealed at 525°C

$[C_{Ag}]$, at %	Average roughness R_a, μm	Root mean square roughness R_{rms}, μm	Skewness R_{sk}	Kurtosis R_{ku}
0	0.23	0.29	0.38	3.12
1.2	0.22	0.27	0.27	2.68
1.9	0.31	0.38	0.34	2.51
2.9	0.20	0.28	1.86	9.65

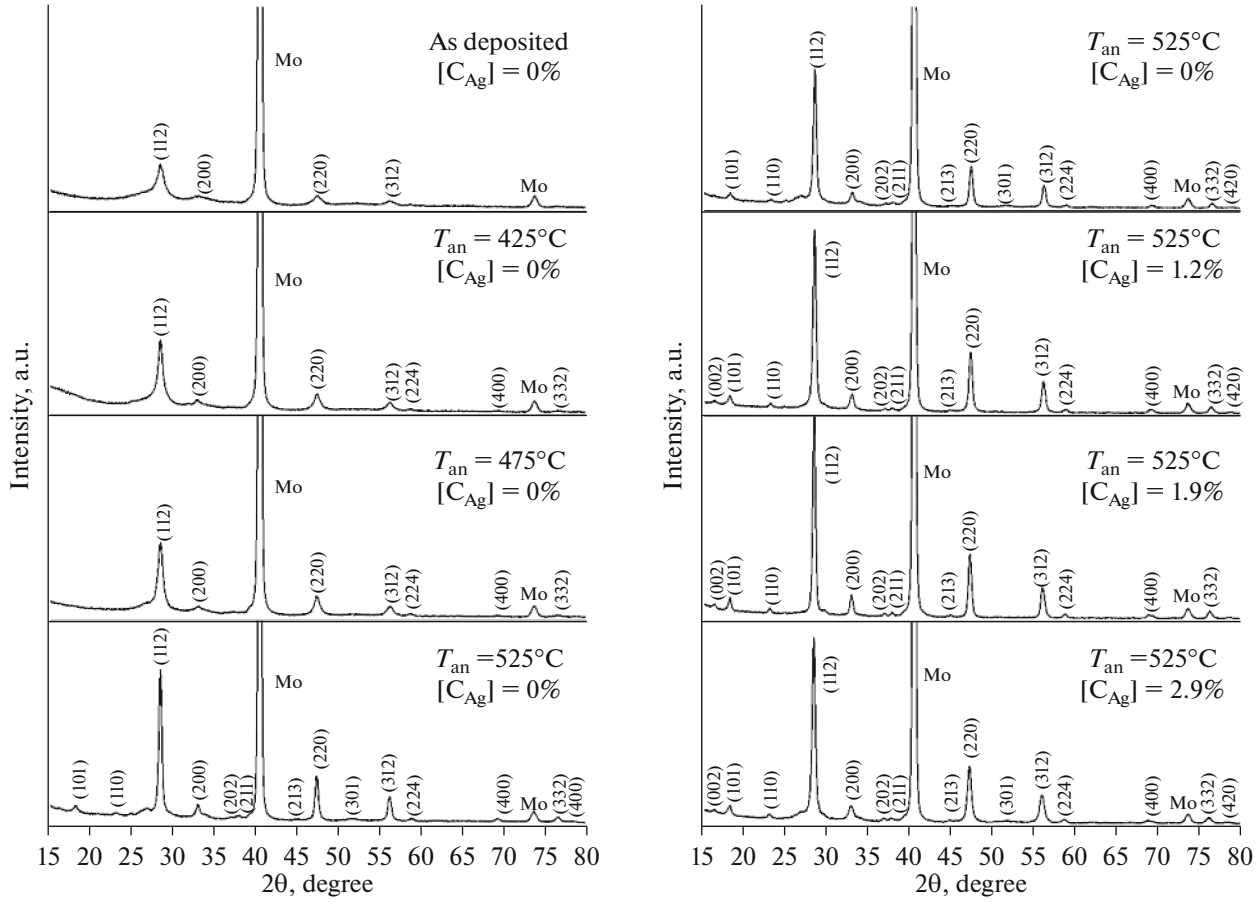

Fig. 4. The XRD of Cu_2ZnSnS_4 thin films at various T_{an} and different concentrations of Ag-alloying.

kurtic distribution and hence it has relatively many high peaks and low pits. But when concentrations of Ag are equal to 1.2 and 1.9%, the films are characterized by the kurtosis parameter $R_{ku} < 3$ and the surface has a platycurtic distribution, with relatively few high peaks and low pits.

The asymmetry and kurtosis parameters are high for samples with an alloying Ag concentration of 2.9%. This is possibly a high concentration of alloying already, leading to a change in the nature of the film surface.

Figure 4 shows the diffraction patterns of thin films for different temperatures annealing and concentrations of Ag.

Many peaks are observed in the range 2θ 10°–80° indicating the crystal structure of the films. The highest-intensity peak on the graphs observed at 2θ ≈ 41.0°, as well as at 2θ ≈ 73.8°, belongs to molybdenum [23]. The other peaks found at 2θ ≈ 18.3°, 23.2°, 33.1°, 37°, 37.9°, 44.95°, 51.05°, 58.85°, 69.1°, 78.7° are associated with the (101), (110), (200), (202), (211), (213), (301), (224), (400), (420) planes of the tetragonal crystal structure for kesterite Cu_2ZnSnS_4 described in the available literature [ICSD card no 01–075–4122].

The highest-intensity peak at 2θ ≈ 28.55° can correspond to the (112) plane of the tetragonal structure of kesterite CZTS, as well as the tetragonal structure of Cu_2SnS_3, cubic or hexagonal structure of ZnS, CuS, and Sn_2S_3. The peak at 2θ ≈ 47.45° can belong to the (220) CZTS plane and to the Cu_2SnS_3 tetragonal structure or cubic structure of ZnS [23–26]. Since most of the lines belong to the tetragonal kesterite structure CZTS, it can be concluded that the films crystallize in this structure.

The number of peaks observed in the range of diffraction angles 2θ from 10° to 80°, as well as their intensity, increases with a growth in the annealing temperature, indicating the improved perfection of the crystal structure of films.

As can be seen (Fig. 4), alloying with Ag introduces no changes in the phase composition of the obtained materials.

The Miller indices (hkl) were identified from the obtained diffraction patterns. Using Gaussian approximation (Origin software), the full width of the peaks at half maximum (FWHM) was found and used to cal-

Table 5. Structural parameters of Cu_2ZnSnS_4 thin films without Ag-alloying

T_{an}, °C	2θ, °	*hkl*	FWHM, radians	*L*, nm	*d*, Å	*a*, Å	*c*, Å	$\delta \times 10^{15}$, lines/m^2	$\varepsilon \times 10^{-2}$
as deposited	28.60	112	0.019	7.4	3.12	5.40 ± 0.02	10.82 ± 0.04	18.3	2.0
425	28.62	112	0.015	9.7	3.12	5.41 ± 0.02	10.76 ± 0.04	10.6	1.5
475	28.59	112	0.014	10.2	3.12	5.41 ± 0.02	10.78 ± 0.04	9.6	1.4
525	28.56	112	0.008	17.9	3.12	5.41 ± 0.02	10.82 ± 0.04	3.1	0.8

Table 6. Structural parameters of Cu_2ZnSnS_4 thin films annealed at 525°C

$[C_{Ag}]$, at %	2θ, °	*hkl*	FWHM, radians	*L*, nm	*d*, Å	*a*, Å	*c*, Å	$\delta \times 10^{15}$, lines/m^2	$\varepsilon \times 10^{-2}$
0	28.56	112	0.008	17.8	3.12	5.41 ± 0.02	10.82 ± 0.04	3.1	0.8
1.2	28.54	112	0.008	17.8	3.12	5.42 ± 0.02	10.81 ± 0.04	3.2	0.8
1.9	28.46	112	0.007	19.6	3.13	5.42 ± 0.02	10.87 ± 0.04	2.6	0.7
2.9	28.43	112	0.009	16.4	3.13	5.43 ± 0.02	10.89 ± 0.04	3.7	0.9

culate such structural parameters of the crystal lattice as interplanar distance (*d*), lattice constants (*a*, *c*), size of the coherent scattering region (*L*), dislocation density (δ) and internal lattice deformation (ε).

The interplanar distance (*d*) was calculated according to the Bragg diffraction law:

$$d = \frac{n\lambda}{2\sin\theta}, \quad (1)$$

where *n*—integer; λ—wavelength of the incident Cu*K*α radiation; θ—Bragg angle.

Since all the main peaks of the CZTS films were associated with a tetragonal structure, the lattice constants are "*a*, *c*" ($a = b \neq c$, $\alpha = \beta = \gamma = 90°$) may be calculated using the following equation:

$$\frac{1}{d^2} = \left[h^2 + k^2 + l^2\left(\frac{a}{c}\right)^2\right]\frac{1}{a^2}. \quad (2)$$

The corresponding values of the constants "*a*, *c*" for the tetragonal lattice calculated from the diffraction patterns are in a good agreement with the theoretical parameters [20].

A size of the coherent scattering region (L) was estimated using the Debye-Scherrer formula [27]:

$$L = \frac{0.94\lambda}{\beta\cos\theta}, \quad (3)$$

where $\beta = \left(\frac{\pi}{4\ln 2}\right)^{\frac{1}{2}}$ FWHM.

The dislocation density (δ) was calculated using the Williamson-Smallman ratio [27]:

$$\delta = \frac{1}{L^2}. \quad (4)$$

The lattice strain (ε) was found using the following ratio [27]:

$$\varepsilon = \frac{\beta}{4\tan\theta}. \quad (5)$$

The structural parameters of CZTS thin films are given in Tables 5 and 6.

The coherent scattering region L grows as the annealing temperature increases, and the interplanar spacing *d* remains invariable (Table 5). Values of the dislocation density δ and of the microdeformation ε decrease as the heat treatment temperature increases, possibly indicating lower defectiveness of the structure. With an increase in the concentration of Ag-alloying, these parameters do not change significantly (Table 6).

The calculated values of the crystal structural parameters reveal practically no change with a growth of the annealing temperature and Ag concentration and are close to the theoretical data [24, 28]. An important result of this work is the demonstration (Tables 5 and 6) that annealing of CZTS films, deposited by spray pyrolysis, in an S_2 atmosphere at 525°C makes it possible to synthesize CZTS films of sufficient structural quality. CZTS films annealed at this temperature have a low values of dislocation density and of lattice strain. What is more, at a small specific dose of substitution of Ag for Cu, the kesterite structure does not change, the values of dislocation density and lattice deformation do not increase, size of the coherent scattering region does not decrease.

Table 7 shows a comparison of some structural parameters of Ag-containing CZTS thin films, obtained in this work by spray pyrolysis, with the literature data. Comparison of different implementations of deposition of metal precursors with subsequent sul-

Table 7. Parameters of CZTS thin films obtained by different synthesis methods

Parameter	This work	Literature data				
		Sputtering and sulfurization [29]	Sputtering and sulfurization [30]	Solvothermal method [31]	Sol-gel method [32]	Electrodeposition technique [33]
a, Å	5.43	–	5.45	5.42	5.43	5.41
c, Å	10.89	–	10.88	10.85	10.85	10.85
d, Å	3.13	–	3.16	–	–	–
Root mean square roughness R_{rms}, μm	0.28	0.18	0.20	–	–	–
(Ag + Cu)/(Zn + Sn) ratio	0.74	0.47	1.15	0.95	0.78	0.93
Stoichiometric ratio (Cu + Zn + Sn + Ag)/S	1.04	0.95	1.25	1.06	1.15	0.68

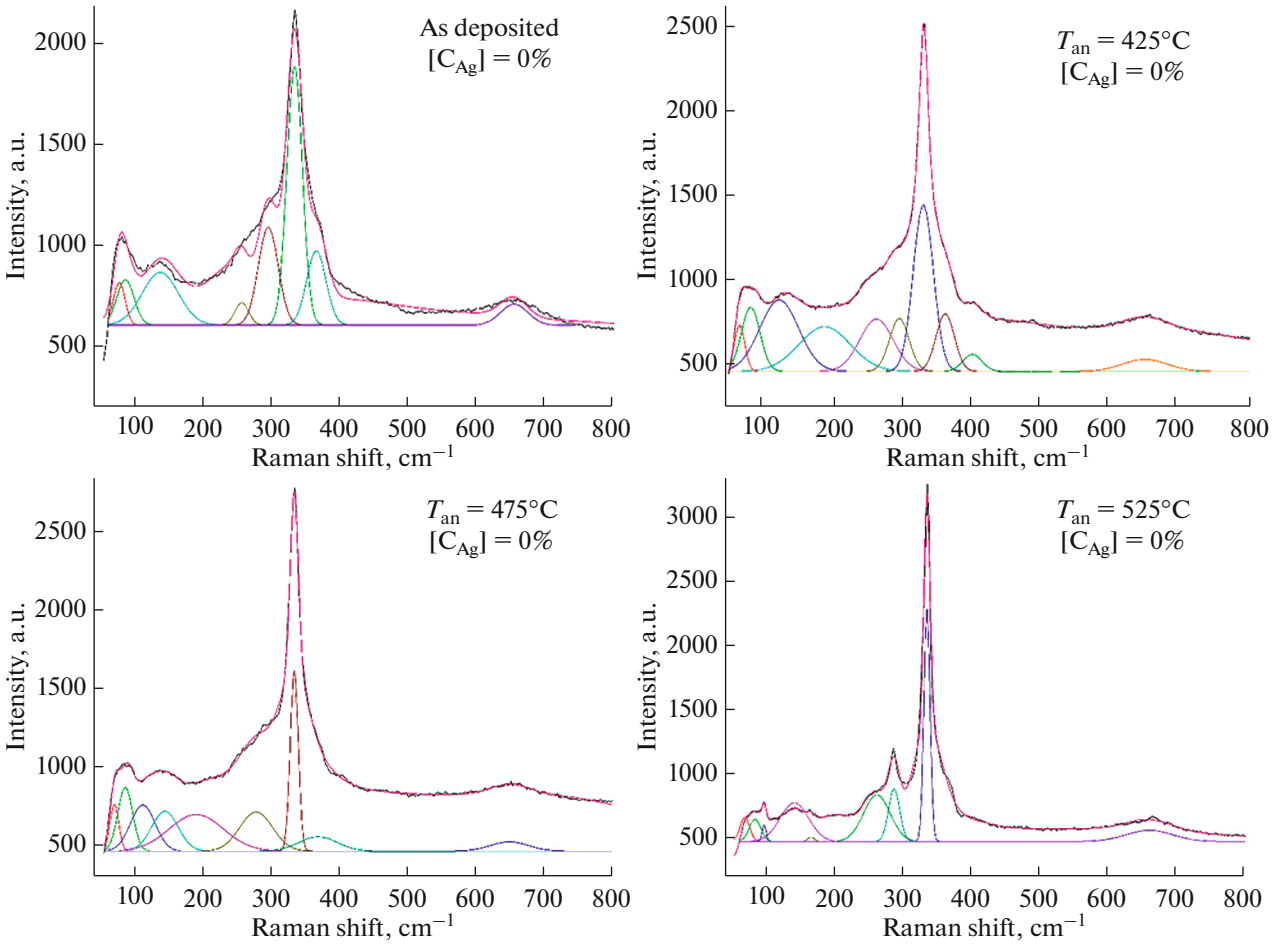

Fig. 5. Raman spectra of Cu_2ZnSnS_4 thin films without Ag-alloying at various T_{an}.

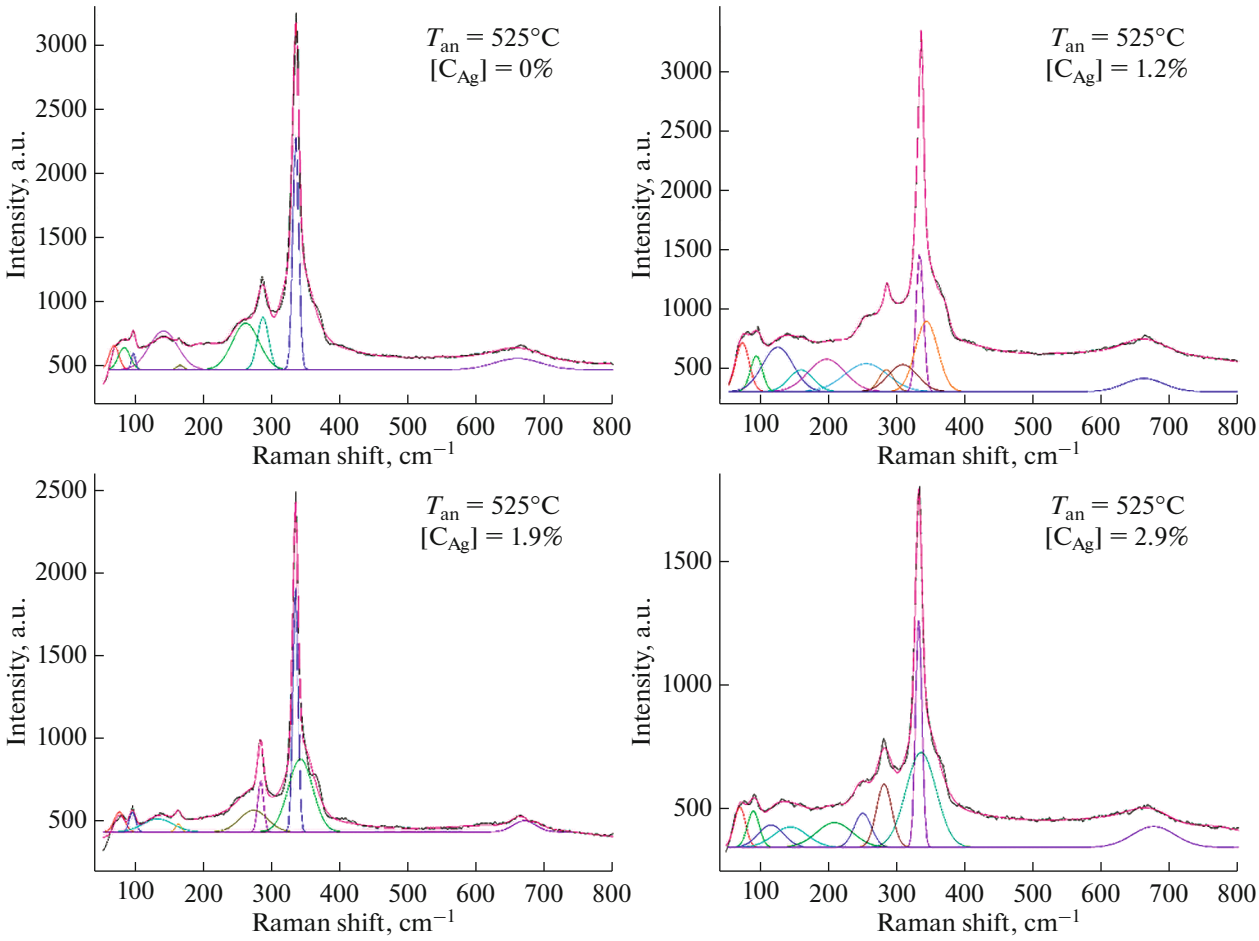

Fig. 6. Raman spectra of Cu_2ZnSnS_4 thin films at T_{an} = 525°C and various concentrations of Ag alloying.

furization [29, 30], solvothermal method [31], sol-gel method with dip-coating technique [32] and electrodeposition technique [33] indicates that the spray pyrolysis method and its parameters used in our work for deposition is suitable for obtaining CZTS films of sufficient structural quality.

CZTS thin films were analyzed by Raman spectroscopy to confirm the formation of the kesterite phase and to detect the presence of secondary phases in the films. Figures 5 and 6 show the obtained Raman spectra, where the envelope line is a sum of the spectral lines approximated by the Lorentz function. The obtained spectra of the films have three main Raman bands at about 286–289, 334–336, and 670–672 cm^{-1}, corresponding to the CZTS compound. The peaks detected at 69–76, 77–87, 94–98, 120–127, 135–149, 252–257, 341–346 cm^{-1} also belong to the kesterite structure CZTS [23].

Similar to the results of X-ray diffraction analysis, some lines may belong not only to the kesterite structure CZTS, but also to some others, e.g. rhombic SnS structure, cubic Cu_2SnS_3, tetragonal Cu_2SnS_3, hexagonal SnS_2, cubic ZnS, CuSn, ZnCuSn [23, 34–36].

Experimental data for the detected lines are presented in Table 8.

Because almost all of the identified bands belong to the kesterite structure CZTS, we can conclude that the films crystallize in the CZTS structure. The data obtained correlate well with those obtained using the method of X-ray phase analysis.

CONCLUSIONS

This paper presents a study into the effect of the heat treatment temperature (20, 425, 475, 525°C) and the concentration of Ag-alloying (0, 1.2, 1.9, 2.9%) on the elemental composition, structure and morphology of Cu_2ZnSnS_4 thin films formed by spray pyrolysis. The analysis was carried out using such standard methods, such as electron microanalysis, scanning probe microscopy, scanning electron microscopy, X-ray diffraction analysis, Raman scattering of light.

Table 8. Observable lines of Raman scattering for Cu_2ZnSnS_4 thin films

Experimental data														Literature data [23, 34–36]				
as deposited $[C_{Ag}] = 0\%$		$T_{an} = 425°C$, $[C_{Ag}] = 0\%$		$T_{an} = 475°C$, $[C_{Ag}] = 0\%$		$T_{an} = 525°C$, $[C_{Ag}] = 0\%$		$T_{an} = 525°C$, $[C_{Ag}] = 1.2\%$		$T_{an} = 525°C$, $[C_{Ag}] = 1.9\%$		$T_{an} = 525°C$, $[C_{Ag}] = 2.9\%$		CZTS	CuSn/ ZnS	ZnCuSn	Cu_2SnS_3/ Cu_3SnS_4	SnS/ SnS_2
PC, cm^{-1}	FWHM, cm^{-1}	PC, cm^{-1}	FWHM, cm^{-1}	PC, cm^{-1}	FWHM, cm^{-1}	PC, cm^{-1}	FWHM, cm^{-1}	PC, cm^{-1}	FWHM cm^{-1}	PC, cm^{-1}	FWHM, cm^{-1}	PC, cm^{-1}	FWHM, cm^{-1}	PC, cm^{-1}	PC, cm^{-1}	PC, cm^{-1}	PC, cm^{-1}	PC, cm^{-1}
77	20	71	18	71	15	69	17	74	23			76	19	68				
86	30	87	31	87	25	85	20			78	18			82				
						98	7	94	21	97	11	95	20	97				
		127	65	112	42	143	49	126	53	135	52	120	43	140				
136	63			145	46							149	57	151				
						166	11	160	42	165	10			164				160
		192	86	192	93			199	63									190
												214	61					219
256	24							257	75			252	29	255				
		265	56			264	46			273	48			266/271	268/275	266	267	
				278	56	289	19	286	26	285	10	285	26	287/275	283	288		
295	34	299	33											302			303	
								310	51					316			318	314
334	27	334	34	335	14	337	11	335	13	336	9	335	11	331/338		338	337	
								346	39	346	42	341	52	342/347				
365	33	365	31	373	66									366/370/ 374	375	372		
659	47	658	75	656	65										663			
						670	81	671	68	672	39	670	73	671				

As revealed by the methods of electron microanalysis, scanning electron microscopy and scanning probe microscopy:

• with an increase in the annealing temperature from 425 to 525°C, the metal/chalcogen ratio changes from 1.59 to 1.06, approaching the stoichiometry, and shows no changes with the addition of Ag as an alloying element;

• under all modes of synthesis, the films have a continuous surface, there are no cracks and voids;

• the average roughness is about 0.2–0.3 μm, and the root-mean-square roughness is about 0.3–0.4 μm for all synthesis modes.

At the same time, these topographic parameters reveal no particular dependence on the heat treatment temperature and the concentration of Ag-alloying.

X-ray diffraction analysis revealed lines at $2\Theta \approx$ 18.3°, 23.2°, 33.1°, 37°, 37.9°, 44.95°, 51.05°, 58.85°, 69.1°, 78.7° corresponding to planes (101), (110), (200), (202), (211), (213), (301), (224), (400), (420) for the tetragonal crystal structure of kesterite Cu_2ZnSnS_4. The lines observed at $2\Theta \approx 28.55°$, 47.45°, 56.2°, 76.4° can belong both to the Cu_2ZnSnS_4 kesterite structure ((112), (220), (312), and (332) planes, respectively) and to the secondary phases of Cu_2SnS_3, ZnS, CuS and Sn_2S_3. As the films are annealed, the number of peaks attributed to kesterite CZTS increases, their intensity increases, FWHM decreases, and the calculated value of the coherent scattering region increases (from 7.4 to 17.9 nm) to indicate an improvement in crystallinity of the films. Since no peaks belonging to other phases were not found, this fact may be an indication of crystallization of the studied films in the tetragonal structure of kesterite Cu_2ZnSnS_4.

The Raman scattering method revealed lines at ~69–74, 85–87, 95–97, 135–149, 252–257, 286–289, 334–336, 341–346 and 670–672 cm^{-1}, which, according to the known literature data, are associated with the Cu_2ZnSnS_4 compound. This agrees with the results of X-ray diffraction analysis and allows us to conclude that the films crystallize in the structure of kesterite Cu_2ZnSnS_4.

Thus, Cu_2ZnSnS_4 films produced by spray pyrolysis, annealed at temperatures of 20, 425, 475, 525°C and alloyed with Ag at the concentrations 0, 1.2, 1.9, 2.9%, have a uniform phase composition. Such topographic parameters as arithmetic roughness and root mean square roughness have rather high values. Alloying with Ag in the selected range of its concentrations has no effect on the phase composition and morphology of the synthesized films, which allows one to apply the synthesis methods, used for pure kesterites, to Ag-containing Cu_2ZnSnS_4 thin films production as well.

ACKNOWLEDGMENTS

The authors from the Belarusian State University appreciate the financial support from State Research Program of the Republic of Belarus "Material Science, New Materials and Technologies".

The authors from the Institute of Applied Physics appreciate the financial support from the European Projects:

• INFINITE-CELL H2020-MSCA-RISE-2017-777968 (2017–2022) INTERNATIONAL COOPERATION FOR THE DEVELOPMENT OF COST-EFFICIENT KESTERITE/C-SI THIN FILM NEXT GENERATION TANDEM SOLAR CELLS.

• ANCD 20.80009.5007.03 (2020–2023) PHOTOVOLTAIC AND PHOTONIC DEVICES WITH ACTIVE ELEMENTS FROM NEW CHALCOGHENIC MATERIALS OBTAINED THROUGH ECONOMICALLY ACCESSIBLE TECHNOLOGIES.

• ANCD 22.80013.5007.5BL (2022–2023) Cu_2ZnGeS_4, Cu_2CdGeS_4 COMPOUNDS AND $Cu_2Zn_xCd_{1-x}GeS_4$ SOLID SOLUTIONS: SYNTHESIS, GROWTH AND PHYSICO-CHEMICAL PROPERTIES.

CONFLICT OF INTEREST

The authors declare that they have no conflicts of interest.

REFERENCES

1. Hironori Katagiri, Cu_2ZnSnS_4 thin film solar cells, *Thin Solid Films,* 2005, vols. 480–481, pp. 426–432. https://doi.org/10.1016/j.tsf.2004.11.024
2. Larsen, J.K., Larsson, F., Törndahl, T., et al., Cadmium free Cu_2ZnSnS_4 solar cells with 9.7% efficiency, *Thin-Film Solar Cells, Adv. Energy Mater.,* 2019, vol. 9, no. 21, p. 1900439. https://doi.org/10.1002/aenm.201900439
3. Minlin Jiang and Xingzhong Yan, Cu_2ZnSnS_4 thin film solar cells: Present status and future prospects, in *Solar Cells—Research and Application Perspectives,* 2013, ch. 5. https://doi.org/10.5772/50702
4. Yusupov, A., Adambaev, K., Turaev, Z.Z., Some electrical and photoelectric characteristics that are promising for photoconverters *p*-Cu_2ZnSnS_4/*n*-Si heterostructures, *Appl. Sol. Energy,* 2015, vol. 51, no. 4, pp. 311–313. https://doi.org/10.3103/S0003701X15040209
5. Li, W., Liu, X., and Cui, H., et al., The role of Ag in $(Ag,Cu)_2ZnSnS_4$ thin film for solar cell application, *J. Alloys Compd.,* 2015, vol. 625, pp. 277–283. https://doi.org/10.1016/j.jallcom.2014.11.136
6. Razykov, T.M., Ergashev, B.A., Yuldoshov, R.T., et al., Production and characteristics of $(ZnSe)_{0.1}(SnSe)_{0.9}$ films for use in thin film solar cells, *Appl. Sol. Energy,* 2018, vol. 54, pp. 255–260. https://doi.org/10.3103/S0003701X18040138
7. Bitam, H., Zaidi, B., Hadjoudja, B., et al., Junction configuration effects on the photovoltaic parameters of

a-Si/Cu_2ZnSnS_4 solar cells, *Appl. Sol. Energy,* 2022, vol. 58, pp. 198–202. https://doi.org/10.3103/S0003701X22020025

8. Mohamed M.A. Abusnina, Synthesis and characterization of kesterite Cu_2ZnSnS_4 (CZTS) thin films for solar cell application, Electronic Theses and Dissertations, 2016, 1153. https://digitalcommons.du.edu/etd/1153.
9. Thi Hiep Nguyen, Takato Kawaguchi, Jakapan Chantana, et al., Structural and solar cell properties of a Ag-containing Cu_2ZnSnS_4 thin film derived from spray pyrolysis, *ACS Appl. Mater. Interfaces,* 2018, vol. 10, pp. 5455–5463. https://doi.org/10.1021/acsami.7b14929
10. Chang Yan, Jialiang Huang, Kaiwen Sun, et al., Efficiency improvement of high band gap Cu_2ZnSnS_4 solar cell achieved by silver incorporation, *2018 IEEE 7th World Conference on Photovoltaic Energy Conversion (WCPEC) (A Joint Conference of 45th IEEE PVSC, 28th PVSEC and 34th EU PVSEC),* 2018. https://doi.org/10.1109/PVSC.2018.8547906
11. Sanchez, M.F., Sanchez, T.G., Courel, M., et al., Effect of post annealing thermal heating on Cu_2ZnSnS_4 solar cells processed by sputtering technique, *Sol. Energy,* 2022, vol. 237, pp. 196–202. https://doi.org/10.1016/j.solener.2022.04.002
12. Xiaojie Yuan, Jianjun Li, and Jialiang Huang, 10.3% Efficient green Cd-free Cu_2ZnSnS_4 solar cells enabled by liquid-phase promoted grain growth, *Small,* 2022, vol. 18, p. 220392. https://doi.org/10.1002/smll.202204392
13. Ahmed Mourtada Elseman and Rashad, M.M., Influence of nitrogen atmosphere one-step heating assisted the solution processing of Kesterite Cu_2ZnSnS_4 as hole extraction on the efficacy of the inverted perovskite solar cells, *Opt. Mater.,* 2022, vol. 124, p. 111998. https://doi.org/10.1016/j.optmat.2022.111998
14. Maryam Heidariramsheh, Mozhdeh Forouzandeh, Nima Taghavinia, and Seyed Mohammad Mahdavi, Effect of Zn/Sn ratio on perovskite solar cell performance applying off-stoichiometric Cu_2ZnSnS_4/carbon hole-collecting electrodes, *ACS Appl. Mater. Interfaces,* 2022, vol. 14, pp. 17296–17311. https://doi.org/10.1021/acsami.2c00206
15. Petukhov, V.Yu. and Gumarov, G.G., Ion-Beam Methods for Obtaining Thin Films, 2010.
16. Lokhande, A.C., Chalapathy, R.B.V., Mingrui He, et al., Development of Cu_2SnS_3 (CTS) thin film solar cells by physical techniques: A status review, *Sol. Energy Mater. Sol. Cells,* 2016, vol. 153, pp. 84–107. https://doi.org/10.1016/j.solmat.2016.04.003
17. Nikale, V.M., Shinde, S.S., Babar, A.R., et al., (Photo) electrochemical investigations on spray deposited *n*-$CdIn_2Se_4$ thin film/polysulphide/c photoelectrochemical solar cell, *Appl. Sol. Energy,* 2010, vol. 46, pp. 194–201. https://doi.org/10.3103/S0003701X10030084
18. Binwen Chen, Guilin Chen, Weihuang Wang, et al., Magnetron sputtering deposition of GeSe thin films for solar cells, *Sol. Energy,* 2018, vol. 176, pp. 98–103. https://doi.org/10.1016/j.solener.2018.10.030
19. You, X., Yanchan Huang, Zhigao Xie et al., Ag alloying for modifications of carrier density and defects in Zn-rich $(Ag,Cu)_2ZnSnSe_4$ thin film solar cells, *J. Alloys Compd.,* 2020, vol. 842, p. 155884. https://doi.org/10.1016/j.jallcom.2020.155884
20. Timmo, K., Altosaar, M., Pilvet, M., et al., The effect of Ag alloying of $Cu_2(Zn,Cd)SnS_4$ on the monograin powder properties and solar cell performance, *J. Mater. Chem. A,* 2019, vol. 7, pp. 24281–24291. https://doi.org/10.1039/C9TA07768E
21. Raj, C.S.A., Sebastian, S., and Susai Rajendran, A review on spray pyrolysis deposited CZTS thin films for solar cell applications, *J. Univ. Shanghai Sci. Technol.,* 2021, vol. 23, no. 9, pp. 1196–1206. https://doi.org/10.51201/JUSST/21/09681
22. Dermenji, L., Guc, M., Gurieva, G., et al., Thin films of $(Ag_xCu_{1-x})_2ZnSn(S,Se)_4$ ($x = 0.05–0.20$) prepared by spray pyrolysis, *Thin Solid Films,* 2019, vol. 690, p. 137532. https://doi.org/10.1016/j.tsf.2019.137532
23. Fernandes, P.A., Salomé, P.M.P., and da Cunha, A.F., Study of polycrystalline Cu_2ZnSnS_4 films by Raman scattering, *J. Alloys Compd.,* 2011, vol. 509, pp. 7600–7606. https://doi.org/10.1016/j.jallcom.2011.04.097
24. ICSD card no. 01-075-4122.
25. Altowairqi, Y., Alsubaie, A., Stroh, K.P., et al., The effect of annealing conditions: Temperature, time, ramping rate and atmosphere on nanocrystal Cu_2ZnSnS_4 (CZTS) thin film solar cell properties, *Mater. Today: Proc.,* 2019, vol. 18 (2), pp. 473–486. https://doi.org/10.1016/j.matpr.2019.06.234
26. Tulshi Shiyani, Malkesh Patel, Indrajeet Mukhopadhyay, and Abhijit Ray, Effect of annealing on structural properties of electrodeposited CZTS thin films, *IETE Technical Review,* 2016, vol. 33, no. 1, pp. 2–6. https://doi.org/10.1080/02564602.2015.1045044
27. Purohit, A., Chander, S., Nehra, S.P., and Dhaka, M.S., Effect of air annealing on structural, optical, morphological and electrical properties of thermally evaporated CdSe thin films, *Phys. E,* 2015, vol. 69, pp. 342–348. https://doi.org/10.1016/j.physe.2015.01.028
28. Kang Gu, Ruiting Hao, Jie Guo, et al., Improved solution processed Cu_2ZnSnS_4 solar cells using a temporary Ag layer, *J. Mater. Sci.: Mater. Electron.,* 2019, vol. 30, pp. 20443–20450. https://doi.org/10.1007/s10854-019-02383-w
29. Gour, K.S., Singh, O.P., Tawale, J.S., and Singh, V.N., Silver (Ag) incorporated Cu_2ZnSnS_4 thin film for improved optical and morphological properties, *Superlattices Microstruct.,* 2018, vol. 120, pp. 54–59. https://doi.org/10.1016/j.spmi.2018.05.012
30. Nagabhushan Jnaneshwar Choudhari, Raviprakash, Y., Bellarmine, F., et al., Investigation on the sulfurization temperature dependent phase and defect formation of sequentially evaporated Cu-rich CZTS thin films, *Sol. Energy,* 2020, vol. 201, pp. 348–

361.
https://doi.org/10.1016/j.solener.2020.03.007

31. Kannan, A.G., Manjulavalli, T.E., and Chandrasekaran, J., Influence of solvent on the properties of CZTS nanoparticles, *Procedia Eng.,* 2016, vol. 141, pp. 15–22.
https://doi.org/10.1016/j.proeng.2015.08.1112
32. Ahmed Ziti, Bouchaib Hartiti, Hicham Labrim, et al., Effect of copper concentration on physical properties of CZTS thin films deposited by dip-coating technique, *Appl. Phys. A,* 2019, vol. 125, p. 218.
https://doi.org/10.1007/s00339-019-2513-0
33. Haribhau Borate, Ajinkya Bhorde, and Ashish Waghmare, Single-step electrochemical deposition of CZTS thin films with enhanced photoactivity, *ES Mater. Manuf.,* vol. 11, pp. 30-39, 2021.
https://doi.org/10.30919/esmm5f934
34. Dimitrievska, M., Fairbrother, A., Fontané, X., et al., Multiwavelength excitation Raman scattering study of polycrystalline kesterite Cu_2ZnSnS_4 thin films, *Appl. Phys. Lett.,* 2014, vol. 104, p. 021901.
https://doi.org/10.1063/1.4861593
35. Cheng, A.-J., Manno, M., Khare, A., Leighton, C., Campbell, S.A., et al., Imaging and phase identification of Cu_2ZnSnS_4 thin films using confocal Raman spectroscopy, *J. Vac. Sci. Technol. A,* 2011, vol. 29, p. 051203.
https://doi.org/10.1116/1.3625249
36. Windom, B.C., Sawyer, W.G., and Hahn, D.W., A Raman spectroscopic study of MoS_2 and MoO_3: Applications to tribological systems, *Tribol. Lett.,* 2011, vol. 42, pp. 301–310.
https://doi.org/10.1007/s11249-011-9774-x